RSC Advances

ROYAL SOCIETY OF CHEMISTRY

www.rsc.org/advances

Graphical Abstract

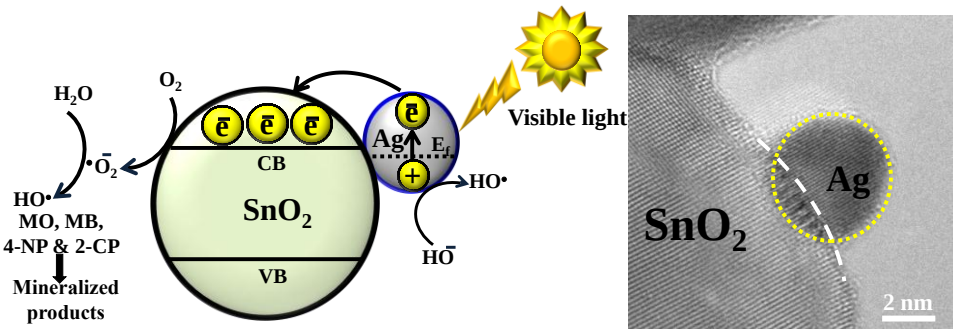

Journal Name

RSC Publishing

ARTICLE

Visible light-driven photocatalytic and photoelectrochemical studies of *Ag*-SnO_2 nanocomposites synthesized using an electrochemically active biofilm†

Cite this: DOI: 10.1039/x0xx00000x

Received 00th January 2012,
Accepted 00th January 2012

DOI: 10.1039/x0xx00000x

www.rsc.org/

Sajid Ali Ansari, Mohammad Mansoob Khan, Mohd Omaish Ansari, Jintae Lee and Moo Hwan Cho*

Ag-SnO_2 nanocomposites (1 mM and 3 mM) were synthesized in water at room temperature using an electrochemically active biofilm. The resulting nanocomposites were characterized by X-ray diffraction, transmission electron microscopy, diffuse reflectance spectroscopy, photoluminescence spectroscopy and X-ray photoelectron spectroscopy. The *Ag*-SnO_2 nanocomposites exhibited enhanced photocatalytic activity under visible light irradiation for the degradation of methyl orange, methylene blue, 4-nitrophenol and 2-chlorophenol compared with pure SnO_2 nanostructures. Photoelectrochemical measurements, such as electrochemical impedance spectroscopy, linear scan voltammetry and differential pulse voltammetry in the dark and under visible light irradiation, further supported the visible light activity of the *Ag*-SnO_2 nanocomposites. These results showed that the Ag nanoparticles induced visible light activity and facilitated efficient charge separation in the *Ag*-SnO_2 nanocomposites, thereby improving the photocatalytic and photoelectrochemical performance.

Introduction

Metal oxide photocatalysis has attracted significant attention because of its promising applications in various fields, such as environment remediation by the photodecomposition of hazardous dyes in polluted water, industrial effluents and solar energy conversion.[1-2] Metal oxides, such as TiO_2, ZnO and SnO_2, have been the prime choice for basic research and practical applications owing to their high activity, good stability, low cost, non-toxicity and chemical inertness.[3-6] One drawback of these metal oxides is their wide band-gap, which is illustrated by their absorption of UV light but not in visible light. Consequently, only small region of the solar spectrum can be utilized when these metal oxides are used as a photocatalyst. Because visible light comprises ~43% of the solar spectrum, therefore, a photocatalyst that is active under visible light is needed.[6-8] Accordingly, considerable efforts has been made to develop visible-light-active metal oxide photocatalysts that can make use of radiation in the visible light region.[2-4,6-8] Recently, the synthesis of nanocomposites by combining metal oxides with noble metals has received significant attention.[9] The light harvesting properties of noble metals, such as Ag and Au, have been exploited worldwide by most researchers for the photocatalytic reaction under visible light irradiation. Furthermore, the electrons in noble metals are excited by a surface plasmon resonance phenomenon and are transferred to the conduction band of the metal oxide. The transferred electrons move to the surface of the metal oxide materials and assist in the formation of super-oxide radical anions and hydroxyl radicals, whereas the holes present on the surface of the metals can act as redox centers to initiate the photocatalytic reactions and enhance the photocatalytic efficiency of metal oxides.[9-15]

SnO_2 has attracted increasing attention as an important metal oxide because of its wide range of applications, such as optoelectronic devices and dye sensitized solar cells, owing to its excellent optical and electrical properties.[6,16] SnO_2 normally exhibits high photocatalytic activity under UV light irradiation, and considerable efforts have been made to enhance its photoactivity in the visible region.[6,16] Better processing methods might improve significantly the catalytic performance of SnO_2. Recently, there have been many reports on the synthesis of photoactive noble metal-SnO_2 nanocomposites using a range of synthetic methods. Wi et al.[17] used a solution-based route for the synthesis of Au–SnO_2 hybrid nanostructures, where as You et al.[18] reported a solution-based method to prepare Au-SnO_2 nanostructures and further tested their photocatalytic activity. These reports have shown that noble metal nanoparticles, such as silver nanoparticles (AgNPs) and gold nanoparticles, anchored to the metal oxide surface enhance the

efficiency of the charge-transfer process. On the other hand, most of the methods reported for the synthesis of metal-metal oxide nanocomposite generally use harmful chemicals, whose discharge into the environment affects the biosphere, which might be related to human health issues. Therefore, there is increasing need for a greener route for metal-metal oxide nanocomposite synthesis.

Electrochemically active microorganisms form electrochemically active biofilms (EABs) on solid surfaces and have potential applications in bioenergy and chemical production.[19-21] EABs have attracted considerable attraction in bio electrochemical systems (BESs), such as microbial fuel cells, where they act as a living bioanode that produce an excess of electrons and protons by biologically oxidizing a range of substrates. The flow of these electrons produces a considerable amount of electricity. Recent studies have shown that the EABs can be used to synthesize noble metal nanoparticles, and metal-metal oxide nanocomposites.[2,12,19]

This paper reports the biogenic synthesis of *Ag*-SnO_2 nanocomposites (*Ag*-SnO_2) using an EAB. The as-prepared *Ag*-SnO_2 was used as a highly visible-light-driven photocatalyst towards the degradation of methyl orange (MO), methylene blue (MB), 4-nitrophenol (4-NP) and 2-chlorophenol (2-CP). Photoelectrochemical measurements, such as electrochemical impedance spectroscopy (EIS), linear scan voltammetry (LSV) and differential pulse voltammetry (DPV) in the dark and under visible light irradiation, further supported the visible light activity of the *Ag*-SnO_2 nanocomposites. The photodegradation efficiency and photoelectrochemical responses of the *Ag*-SnO_2 nanocomposites were significantly higher than those of pure SnO_2 (*p*-SnO_2). This study suggests that *Ag*-SnO_2 nanocomposites are promising candidates for photocatalysis and photoelectrode materials.

Experimental

Materials

Silver nitrate ($AgNO_3$, 99% pure), tin oxide nanoparticles (SnO_2), MB and 2-CP were purchased from Sigma–Aldrich. Sodium acetate, MO, 4-NP and sodium sulfate (Na_2SO_4) were obtained from Duksan Pure Chemicals Co. Ltd. South Korea and used as received. α-terpineol and ethyl cellulose were purchased from KANTO Chemical Co., Japan and fluorine-doped transparent conducting oxide glass (FTO; F-doped SnO_2 glass; 7 Ω/sq) was purchased from Pilkington, USA. Carbon paper (without wet proof, Fuel Cell Earth LLC, USA), and all other chemicals used in this study were of analytical grade and used as received. All solutions were prepared in deionized water that was obtained using a PURE ROUP 30 water purification system.

Methods

X-ray diffraction (XRD, PANalytical, X'pert PRO-MPD, Netherland) was carried out using Cu Kα radiation (λ = 0.15405 nm). The XRD peaks of the crystalline phases were compared with those of standard compounds reported in the JCPDS data file. A UV-VIS-NIR spectrophotometer (Cary 5000, VARIAN, USA) was used to record the diffuse reflectance/absorbance spectra (DRS) of the *p*-SnO_2 and *Ag*-SnO_2 nanocomposites (1 mM and 3 mM *Ag*-SnO_2) samples in the range, 200-800 nm. X-ray photoelectron spectroscopy (XPS, ESCALAB 250 XPS System, Thermo Fisher Scientific U.K.) was performed using a monochromatized Al Kα x-ray source (hν = 1486.6 eV). The binding energy of C1s (284.60 eV) was used to calibrate the other binding energies at Korea Basic Science Institute (KBSI). The size and distribution of the *Ag*-SnO_2 and *p*-SnO_2 nanoparticles were observed by field emission transmission electron microscopy (FE-TEM, Tecnai G2 F20, FEI, USA) with an accelerating voltage of 200 kV combined with energy dispersive spectrometry (EDS). The photoluminescence (PL, Kimon, 1 K, Japan) of the samples (*p*-SnO_2 and *Ag*-SnO_2) were recorded over the range, 200-800 nm at KBSI. The photoelectrochemical and photocatalytic experiments were performed using a 400 W lamp with an intensity of 31 mW/cm^2 and λ > 400 nm (3M, USA). EIS and LSV were performed in a three electrode cell with a 0.2 M Na_2SO_4 aqueous solution as the electrolyte using a potentiostat (VersaSTAT 3, Princeton Research, USA). The DPV of the *p*-SnO_2 and *Ag*-SnO_2 nanocomposites photoelectrodes were recorded with a pulse height of 50 mV, pulse width of 0.005s and scan rate of 4 mV/s. The working electrodes were prepared as follows. 100 mg of *p*-SnO_2 and *Ag*-SnO_2 (1 mM and 3 mM) were suspended thoroughly using a conditioning mixer by adding ethyl cellulose as a binder and α-terpineol as a solvent for the paste. The resulting mixture was then coated on a FTO glass electrode using the doctor-blade method. The *p*-SnO_2 and *Ag*-SnO_2-coated (FTO) glass substrates were used as the working electrode. Ag/AgCl (saturated with KCl) and a Pt gauge were used as the reference and counter electrodes.

Electrochemically active biofilm preparation

The EABs were developed on plain carbon paper according to previous studies.[19-21] In a typical procedure, carbon paper with a size of 2.5 cm × 4.5 cm was dipped into a mineral salt medium containing sodium acetate (1 g/ L) as a substrate in a 250 mL bottle. 10 mL of anaerobic sludge (from a biogas plant in Paju, Korea) was added under strict anaerobic conditions by sparging N_2 gas for 5 min to remove environmental oxygen contamination. All media, including the bacterial inoculum, were changed every two days under strict anaerobic conditions. This process was repeated for two weeks, and a living EAB was formed on the surface of the carbon paper.

Synthesis of *Ag*-SnO_2 nanocomposites

The EABs developed on carbon paper were used to synthesize the *Ag*-SnO_2 nanocomposite, as shown in Fig. 1. In a typical process, aqueous solutions of $AgNO_3$ (1 mM and 3 mM) were added to a 200 mL suspension of SnO_2 nanoparticles (4 mM). Subsequently, 0.2 g sodium acetate (1 g/L) was added as an electron donor. The mixture of $AgNO_3$ and SnO_2 nanoparticles was stirred for 5 min to allow the complete adsorption of Ag^+ ions on the *p*-SnO_2 surface. After the complete adsorption of Ag^+ ions on the *p*-SnO_2 surface, EAB was hung in a bottle. EAB produced electrons under anaerobic conditions, resulting in the reduction of Ag^+ ions on the *p*-SnO_2 surface. The color change after 12 h indicated the formation of *Ag*-SnO_2 in the

solution, which was centrifuged to isolate the *Ag*-SnO_2. The isolated *Ag*-SnO_2 was dried in an oven at 90 °C for 10 hours, and stored in a desiccator until required.

Two control experiments were further performed to check the role of the EAB and sodium acetate. One was performed in the absence of an electron donor (sodium acetate), in which only the prepared EAB was hung in a SnO_2 and $AgNO_3$ solution under anaerobic conditions. The other controlled experiment was performed in the absence of the EAB by adding only an electron donor (sodium acetate) in a SnO_2 and $AgNO_3$ mixture under anaerobic conditions. In both the controlled experiments, no color change was observed, even after 24 h. These experiments confirmed the role of EAB and acetate in the synthesis of *Ag*-SnO_2 nanocomposites.

Photocatalytic degradation

The photocatalytic activities of the *Ag*-SnO_2 nanocomposites were evaluated by the decomposition of MO, MB, 4-NP and 2-CP under visible light irradiation. 2 mg of each (*p*-SnO_2 and *Ag*-SnO_2) photocatalyst was dispersed in an aqueous solution in two different 20 mL MO (10 mg/L), 20 mL MB (10 mg/L), 20 mL 4-NP (5 mg/L) and 20 mL 2-CP (50 mg/L) solutions, and agitated for 10 min in the dark to achieve adsorption-desorption equilibrium. The above suspensions were irradiated with visible light and after 1 h, a 2 mL sample of the solution was taken and the catalyst was separated from the solution by centrifugation to obtain a clear liquid. The concentrations of MO, MB, 4-NP and 2-CP were analyzed by measuring the absorbance at the characteristic wavelengths using a UV–vis spectrophotometer. The reaction kinetics and decolorization efficiency of the photocatalyst were determined using the method reported elsewhere.[2,6,12]

Photoelectrochemical studies (EIS, LSV and DPV)

To examine the photoelectrochemical response of *p*-SnO_2 and *Ag*-SnO_2, DPV, EIS and LSV experiments were carried out under ambient conditions in the dark and under visible light irradiation. The DPV experiment was carried out under ambient conditions in 50 mL of a 0.2 M phosphate buffer solution (pH = 7), whereas the EIS and LSV experiments were performed in 50 mL of an aqueous 0.2 M Na_2SO_4 solution at room temperature. For each electrode, EIS was first performed in the dark and later under visible light irradiation (λ > 400 nm) at 0.0 V and with a frequency ranging from 1 – 10^4 Hz. The photocurrent response was examined by LSV in the dark and under visible light irradiation at a scan rate of 50 mV/s over a potential range, -0.9 to 1.0 V.

Results and discussion

Proposed reaction mechanism for the synthesis of the *Ag*-SnO_2 nanocomposites

The EAB was used as an innovative and green tool to synthesize the *Ag*-SnO_2 nanocomposites (1 mM and 3 mM), employing a low-cost, surfactant-free and environmentally-friendly method. The EABs provide an excess of electrons and protons by biologically decomposing sodium acetate.[19-21] These electrons reduce Ag^+ ions to Ag^0 at the surface of the SnO_2 nanostructure (Fig. 1). The advantage of this synthesis is that it does not involve external energy input and normally occurs in water at room temperature. This makes the synthesis highly useful and efficient for nanocomposite synthesis.[2,6,12,19,20]

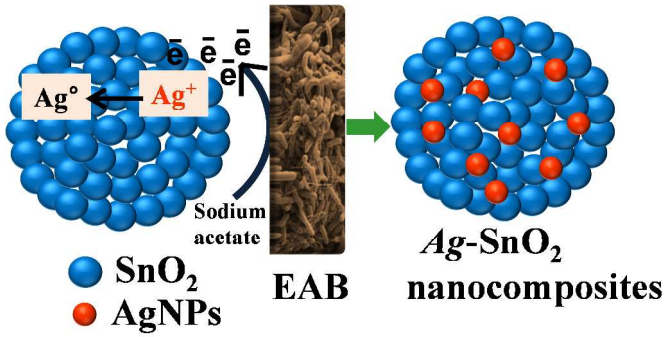

Fig. 1 Schematic diagram of *Ag*-SnO_2 nanocomposites synthesis.

X-ray diffraction analysis

Fig. 2 presents the XRD patterns of *p*-SnO_2, 1 mM and 3 mM *Ag*-SnO_2 nanocomposites. Two sets of XRD patterns were obtained, those unmarked were indexed to the crystalline tetragonal structure of SnO_2 (JCPDS no. 41-1445),[6] whereas the other peaks marked with "*" were assigned to face centered cubic (fcc) Ag (JCPDS no. 04-0783).[2,12,13,17] The absence of any other XRD peaks indicates the high purity of the sample. In addition, the crystallize size calculated using the Scherrer formula, was ~11.00 nm, ~14.20 and 14.57 nm for the *p*-SnO_2, 1 mM and 3 mM *Ag*-SnO_2 nanocomposites, respectively.[2,12,13]A significant change in the crystallite size of the *Ag*-SnO_2 nanocomposites was observed, showing that the small AgNPs had deposited on the surface of the *p*-SnO_2 nanoparticles.

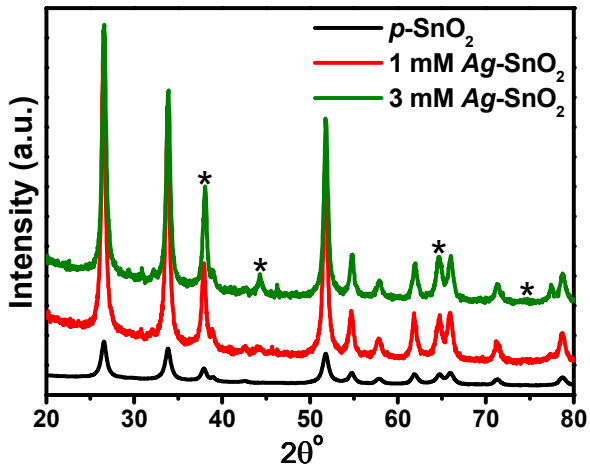

Fig. 2 XRD patterns of *p*-SnO_2, 1 mM and 3 mM *Ag*-SnO_2 nanocomposites. The peaks marked with (*) were assigned to AgNPs.

Optical properties

The light absorption characteristics of *p*-SnO_2, 1 mM and 3 mM *Ag*-SnO_2 nanocomposites were examined by UV-visible diffuse reflectance (Fig. S1) and absorbance spectroscopy (Fig. 3a). The spectrum for *p*-SnO_2 shows that they absorb mainly in the UV range because of their wide band gap. Moreover, the 1 mM and 3 mM *Ag*-SnO_2 nanocomposites showed a broad absorption peak from 400-550 nm, which can be attributed to the surface plasmon resonance absorption of AgNPs.[2,13] This further confirms that AgNPs had been deposited successfully on the *p*-SnO_2 surface. Interestingly, *Ag*-SnO_2 nanocomposites prepared from the silver precursor at different concentrations (1 mM and 3 mM $AgNO_3$) exhibited different and higher absorption intensity in the visible region compared to *p*-SnO_2. The extended absorbance of the *Ag*-SnO_2 nanocomposites in the visible region is expected to improve the photocatalytic activity under sunlight or visible light irradiation. This shift in the absorption spectra of the *Ag*-SnO_2 nanocomposites also suggests an interaction between Ag and *p*-SnO_2, which is also in accordance with the XRD patterns.[2]

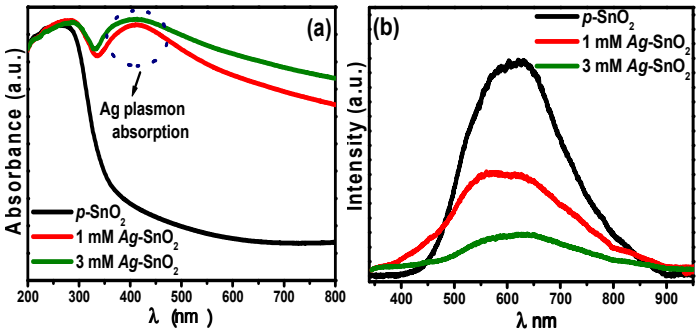

Fig. 3 (**a**) UV-vis diffuse absorption spectra, and (**b**) Photoluminescence spectra of *p*-SnO_2, 1 mM and 3 mM *Ag*-SnO_2 nanocomposites.

Fig. 3b shows the PL spectra of *p*-SnO_2, 1 mM and 3 mM *Ag*-SnO_2 nanocomposites. The intensity of the PL spectrum is related directly to the electron-hole recombination rate, i.e. more the intense the spectrum, the higher the rate of electron-hole recombination.[22] Alternatively, a lower intensity indicates that more excited electrons are trapped and transferred stably through the interface.[2,12,13,22] *p*-SnO_2 exhibits the strongest emission intensity of the PL spectrum, confirming the fastest charge recombination rate, whereas in the case of the 1 mM and 3 mM *Ag*-SnO_2 nanocomposites, the PL intensity was reduced significantly after the anchoring of AgNPs because Ag can trap photo-generated electrons to facilitate charge separation.[2,12-13,22] In general, the efficient charge separation and the inhibited electron-hole recombination by AgNPs are favorable for enhancing the photocatalytic activity of *p*-SnO_2. The PL spectra showed that anchoring the AgNPs to the surface of *p*-SnO_2 can effectively inhibit the electron/hole recombination during a photocatalytic reaction under visible light irradiation.

TEM analysis

The microstructural characteristics of the *p*-SnO_2 and *Ag*-SnO_2 nanocomposites were observed by TEM and HR-TEM. Fig. S2 and S3 shows TEM and HR-TEM images of the *p*-SnO_2 nanoparticles, respectively. Fig. 4 shows the TEM and HR-TEM images of the *Ag*-SnO_2 nanocomposites. As shown in Fig. 4b and 4b', AgNPs with a particle size of ~5-10 nm were attached to the surface of the *p*-SnO_2 nanoparticles. From the HR-TEM image of the *Ag*-SnO_2 nanocomposites, the AgNPs and SnO_2 could be identified clearly by the lattice fringes (Fig. 4c and 4c'). The lattice fringes with d = 0.26 nm spacing were assigned to the Ag (111) planes and the lattice fringes with d = 0.33 nm were assigned to the (110) plane of SnO_2. Furthermore, Fig. 4c and 4c' clearly shows that the AgNPs were attached to the surface of the SnO_2 nanoparticles. The SAED pattern in Fig. S4, S5 and S6 also confirmed the single crystalline nature of the materials. Fig. S7, S8 and S9 show HAADF-STEM images of the *p*-SnO_2, 1 mM and 3 mM *Ag*-SnO_2 nanocomposites, respectively. Fig. S10, S11 and S12 shows the EDX spectra of the *p*-SnO_2, 1 mM and 3 mM *Ag*-SnO_2 nanocomposites, respectively, corresponding to the Sn (K), O (K) and Ag (K) lines. EDX (Fig. S11 and S12) further confirmed the presence of Sn, Ag and O in the samples. These results are in good agreement with the XRD patterns, and show that the *Ag*-SnO_2 nanocomposites has a highly crystalline structure with a small and relatively uniform distribution of AgNPs at the SnO_2 surface.

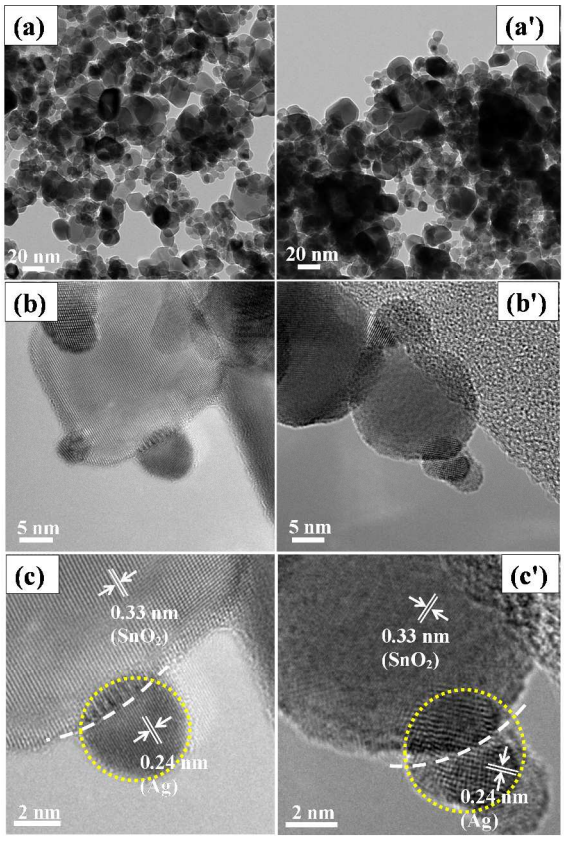

Fig. 4 TEM and HR-TEM images of 1 mM *Ag*-SnO_2 (**a, b** and **c**) and 3 mM *Ag*-SnO_2 nanocomposites (**a', b'** and **c'**).

XPS analysis

XPS was used to examine the chemical states and surface composition of *p*-SnO_2, 1 mM and 3 mM *Ag*-SnO_2 nanocomposites. The XP survey spectra of *p*-SnO_2, 1 mM and 3 mM *Ag*-SnO_2 nanocomposites (Fig. 5a) revealed three major sets of peaks for the Sn 3d peaks, O 1s peaks and Ag 3d peak, which exist in the samples and no trace of any impurity was observed. The carbon peak in Fig. S13 (C 1s = 284.8 eV) was assigned to the residual carbon from the sample and hydrocarbons from the XPS instrument. The high-resolution XP spectra of Sn 3d, O 1s and Ag 3d (Fig. 5b, c and d) showed slightly different binding energies of these electrons in the case of SnO_2, suggesting an interaction between the Ag and SnO_2 nanoparticles. Furthermore, two XPS peaks of the Sn $3d_{5/2}$ and Sn $3d_{3/2}$ core level states of Sn centered at 486.8 and 495.4 eV corresponds to the binding energy of Sn^{4+} in SnO_2.[6] In Fig. 5c, the O 1s spectra of the *p*-SnO_2, 1 mM and 3 mM *Ag*-SnO_2 nanocomposites showed a single symmetrical peak at ~530.46 ± 0.05 eV, corresponding to the lattice oxygen of SnO_2 nanoparticles.[6]

Fig. 5d shows the photoelectron peak of Ag 3d. The Ag 3d photoelectron peaks showed two individual peaks at 367.5 ± 0.02 eV for Ag $3d_{5/2}$ and 373.5 ± 0.02 eV for Ag $3d_{3/2}$.[2,4,13,23] The 6.0 eV difference between the binding energy of these photoelectron peaks is also characteristic of metallic Ag, which is further evidence of the reduction of Ag^{+} ions by the EAB.

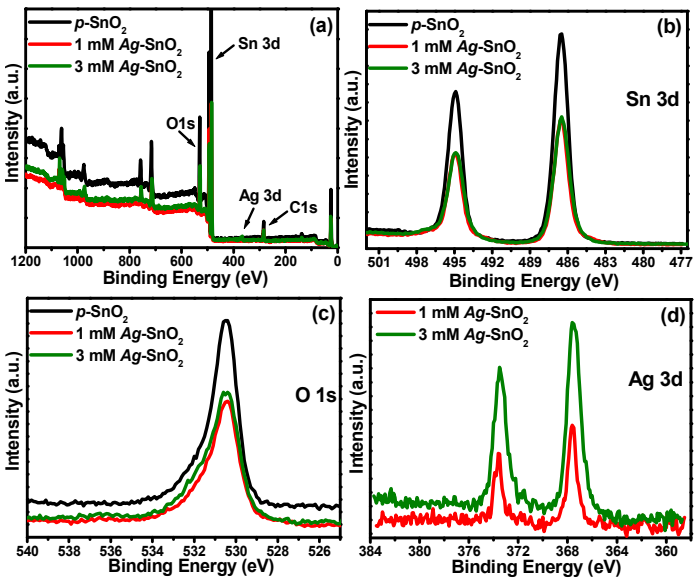

Fig. 5 XP spectra of *p*-SnO_2, 1 mM and 3 mM *Ag*-SnO_2 nanocomposites (**a**) survey spectra (**b**) Sn 3d peaks (**c**) O 1s peaks, and (**d**) Ag 3d peak.

Visible light photocatalytic performance

The photocatalytic activity of the as-prepared *Ag*-SnO_2 nanocomposites (1 mM and 3 mM) were evaluated by the degradation of colored dyes (MO and MB) and non-colored organic compounds (4-NP and 2-CP) as model reaction under visible light irradiation. Fig. 6a, 6b, 6c and 6d shows the photocatalytic degradation kinetics of MO, MB, 4-NP and 2-CP, whereas Fig. S14a, S14b, S14c and S14d show the degradation (C/C_0) of MO, MB, 4-NP and 2-CP as a function of the irradiation time. Here, C is the absorption of MO, MB, 4-NP or 2-CP solution at each time interval of irradiation, and C_0 is the absorption of the initial concentration (time 0). After visible light irradiation on MO and MB for 6 h and 5 h, respectively, almost complete degradation occurred. The change in the concentration of MO and MB as a function of the reaction time for the *p*-SnO_2, 1 mM and 3 mM *Ag*-SnO_2 nanocomposites exhibited pseudo-first-order kinetics according to the equation reported elsewhere.[6] The rate constants (*k*) of the *p*-SnO_2, 1 mM and 3 mM *Ag*-SnO_2 nanocomposites for the degradation of MO were 0.02408/h (R^2 = 0.9956), 0.0894/h (R^2 = 0.9970) and 0.2378/h (R^2 = 0.9879), respectively. Similarly, the rate constants of the *p*-SnO_2, 1 mM and 3 mM *Ag*-SnO_2 nanocomposites for the degradation of MB were 0.05578/h (R^2 = 0.9884), 0.1888/h (R^2 = 0.9987) and 0.2897/h (R^2 = 0.9974), respectively. The *k* value for the visible light degradation of MO and MB by the 3 mM *Ag*-SnO_2 nanocomposites was ~10 and 6 times higher, respectively, than that of *p*-SnO_2. The *Ag*-SnO_2 nanocomposites showed enhanced visible light photocatalytic activity compared to *p*-SnO_2 and other reported metal-metal oxide nanocomposites.[2,12,13]

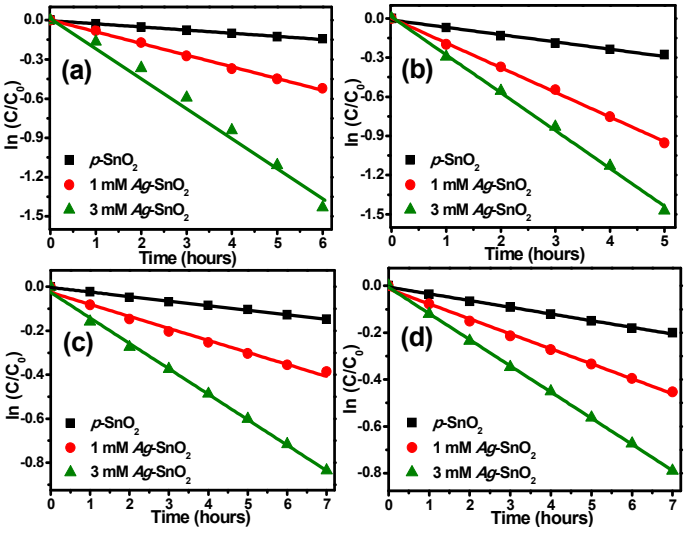

Fig. 6 ln (C/C_0) *versus* time (h) plot for the photodegradation of (**a**) MO, (**b**) MB, (**c**) 4-NP, and (**d**) 2-CP by *p*-SnO_2, 1 mM and 3 mM *Ag*-SnO_2 nanocomposites under visible light irradiation.

Moreover, the sensitization effects of dyes were not excluded because of the absorbance of dyes in the visible region. To further verify this effect, the photocatalytic degradation of non-colored phenolic compound such as 4-NP and 2-CP, which did not absorb the light in the visible region, was also performed under visible light irradiation (Fig 6c, Fig 6d, Fig. S14c and S14d).[24,25] The *k* value of the *p*-SnO_2, 1 mM and 3 mM *Ag*-SnO_2 nanocomposites for the degradation of 4-NP were 0.0207/h (R^2 = 0.9970), 0.0545/h (R^2 = 0.9850) and 0.1157/h (R^2 = 0.9973), respectively. Similarly, the rate constants of the *p*-SnO_2, 1 mM and 3 mM *Ag*-SnO_2 nanocomposites for the degradation of 2-CP were 0.0286/h (R^2 = 0.9970), 0.0638/h (R^2 = 0.9970) and 0.1116/h (R^2 = 0.9997), respectively. The *k* value

for the visible light degradation of 4-NP and 2-CP by the 3 mM *Ag*-SnO_2 nanocomposites was ~6 and 4 times higher, respectively, than that of *p*-SnO_2.The results indicated that the photocatalytic activity was significantly improved by anchoring with AgNPs. The higher observed photocatalytic activity of *Ag*-SnO_2 compared to *p*-SnO_2 suggests that the AgNPs anchored at the surface of *p*-SnO_2 and behave as an electron sink, which increases the separation of the photogenerated electron-hole pairs significantly and inhibits their recombination. This suggests that the AgNPs at the surface of *p*-SnO_2 enhanced the photocatalytic activity of the *p*-SnO_2 for the effective degradation of dyes and other organic pollutants under visible light irradiation.

Mechanism for the degradation of MO and MB

Fig. 7 presents the mechanistic profile of the photoinduced charge separation, migration and degradation process under visible light irradiation. Metal-metal oxide nanocomposites,[26] such as Au-CeO_2[12] and Ag-ZnO,[2,13] can be used as highly-active photocatalysts because of the synergistic effect between the metal oxide and the surface plasmon resonance effect of the noble metal. Generally, a Schottky barrier is formed when two materials with different work functions are combined, and electrons are transferred from the materials with the lower work function to the materials with the higher work function until the two levels reach equilibrium to form a new Fermi energy level.[2,12-13,26] The equilibrium alignment of the Fermi level of the metal and metal oxide nanocomposite materials creates a built-in electric field in the space charge region near the interface, which promotes the separation of photogenerated electrons and holes, and enhances the photocatalytic activity.[2,12,17,26]

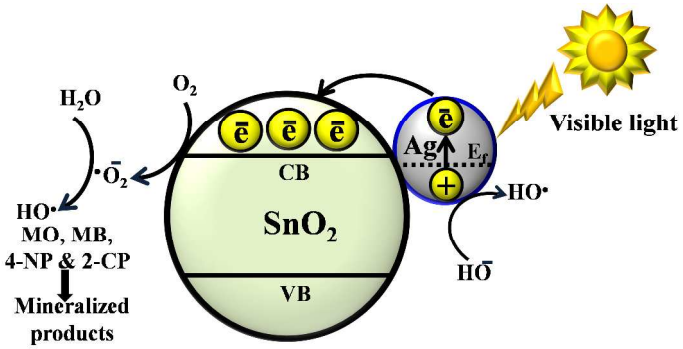

Fig. 7 Schematic diagram of the photocatalytic mechanism for the degradation of MO, MB, 4-NP and 2-CP in the presence of *Ag*-SnO_2 nanocomposites under visible light irradiation.

When subjected to visible-light irradiation, the *Ag*-SnO_2 nanocomposites were excited due to the surface plasmon resonance of the AgNPs, resulting in the generation of electron-hole pairs on the surface of the AgNPs. The photoexcited electrons transfer rapidly occurs from Ag to SnO_2 through the interface between the AgNPs and SnO_2.[2,9,12,13,26,27] These injected electrons are trapped by dissolved oxygen molecules in water to yield a high oxidative species, such as super-oxide radical anions ($^{\bullet}O_2^-$) and hydroxyl radicals ($HO^{\bullet}$).[2,8,12] On the other hand, some of the photoinduced holes on the surface of the AgNPs can be trapped by OH^- to produce $HO^{\bullet}$ species, which is an extremely strong oxidant for the partial or complete mineralization of organic chemicals. The trapping nature of the AgNPs also results in the production of more super oxide radical anions. Super-oxide radical anions ($^{\bullet}O_2^-$) and hydroxyl radicals ($HO^{\bullet}$) produced under visible light irradiation might induce the mineralization of organic pollutants.[2,8,12,28] In general, the photocatalytic activity has a positive correlation with the rate of reactive radical formation, i.e. faster forming radicals leads to a higher photocatalytic activity of the catalyst. Overall, these results suggest that the AgNPs at the surface of the SnO_2 nanoparticles will help increase the rate of formation of $^{\bullet}O^{2-}$ and $HO^{\bullet}$ reactive radicals, facilitating the degradation of organic pollutants.

Photoelectrochemical Studies

Differential pulse voltammetry

DPV was performed to characterize the charging behaviors of the *p*-SnO_2, 1 mM and 3 mM *Ag*-SnO_2 nanocomposites.[29-31] Fig. 8 shows the well-defined quantized capacitance charging peaks in the dark and under visible light irradiation for *Ag*-SnO_2 nanocomposites. The *Ag*-SnO_2 nanocomposites under visible light irradiation exhibited enhanced and excellent charge storage properties compared to *p*-SnO_2. These stored electrons within the nanocomposite were used to form different oxidative species under visible light irradiation, which might be responsible for mineralizing the organic pollutants.

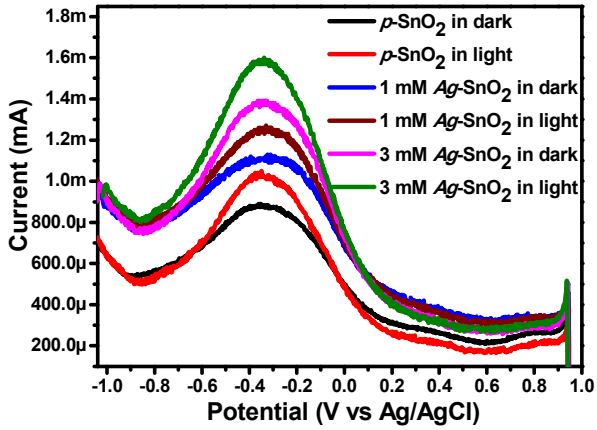

Fig. 8 DPV graph of the *p*-SnO_2 and *Ag*-SnO_2 nanocomposite photoelectrodes in the dark and under visible light irradiation.

EIS measurements

The interface charge separation of the photoelectrons and holes is a critical factor for the photocatalytic activity. To examine the charge separation process and transport properties of the as-prepared *Ag*-SnO_2 nanocomposites as a photoelectrode, EIS was performed in the dark and under visible light irradiation, as shown in Fig. 9a. In general, the complex impedance plot is normally presented as real Z' vs. imaginary Z'', which originate from the resistance and capacitance component of the electrochemical cell. A typical Nyquist plot includes one or more semicircular arcs with the

diameter along the Z' axis. The semicircular arcs observed in the high and low frequency regions correspond to an electron-transfer process, and its diameter represents electron transfer or charge transfer resistance.[32-35] In some cases, the semicircular arc in the high frequency region does not converge and extends as a straight line subtending an angle of 45° to the x-axis, representing a diffusion limited charge transfer process. In the present study, only a semicircular arc with a large diameter was observed for *p*-SnO_2, indicating a very slow electron-transfer process. In particular, a smaller radius of the arc in the EIS spectra indicates a smaller electron transfer resistance at the surface of the photoelectrodes, which normally leads to the more effective separation of the photoelectron-hole pairs and faster interfacial charge transfer. The arc radius of the EIS Nyquist plots of the *Ag*-SnO_2 was smaller than that of the *p*-SnO_2 in the dark and under visible light irradiation, indicating faster interfacial charge transfer at the *Ag*-SnO_2 photocatalyst surface (Fig. 9a). These results show that the interaction between Ag and SnO_2 effectively enhances the separation and transfer efficiency of the photogenerated electron–hole pairs in *Ag*-SnO_2. EIS confirmed that the as-prepared *Ag*-SnO_2 can be used as an effective material for photoelectrodes.

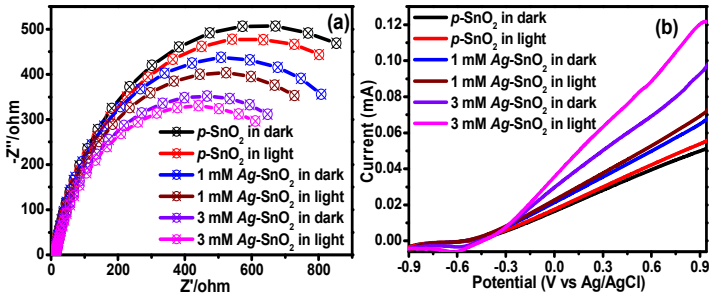

Fig. 9 (**a**) Nyquist plots, and (**b**) Linear scan voltammograms obtained for the *p*-SnO_2 and *Ag*-SnO_2 nanocomposite photoelectrodes in the dark and under visible light irradiation.

Photocurrent measurement

To provide additional evidence for the visible light photocatalytic properties, LSV was performed in the dark and under visible light illumination for the *p*-SnO_2, 1 mM and 3 mM *Ag*-SnO_2 nanocomposites.[2,6,36-41] As shown in Fig. 9b, the *Ag*-SnO_2 nanocomposites under visible light irradiation exhibited a higher photocurrent than *p*-SnO_2. The AgNPs present on the surface of SnO_2 can absorb visible light and generate more photoelectrons due to the SPR phenomenon (Fig. 7). The enhancement of the photocurrent illustrated the increase in the photoinduced carrier transport rate and the improvement in photogenerated electron-hole pair separation. The formation of a Schottky junction at the metal-metal oxide interface can also separate the photoelectrons and holes, and increase the photocurrent.[2,6,36] Furthermore, the extent of electron–hole recombination in the *p*-SnO_2 and *Ag*-SnO_2 was also supported by the photoluminescence (PL) measurements (Fig. 3b). These results show that AgNPs can harvest visible light and effectively suppress the recombination of photogenerated electron-hole pairs; thus enhance the photocatalytic activity of *Ag*-SnO_2. Overall, these results show that *Ag*-SnO_2 can be an effective material for enhancing the photocurrent.

The enhanced performance of the visible light photocatalytic reaction for the degradation of MO and MB, and the photoelectrochemical studies (EIS, LSV and DPV) shown by *Ag*-SnO_2 nanocomposites confirmed that the AgNPs had been deposited on the SnO_2 surface. The interfacial interaction and charge transfer between the AgNPs and SnO_2 could be responsible for the enhanced visible light activities of the *Ag*-SnO_2 nanocomposites.

Stability and reusability of the *Ag*-SnO_2 nanocomposites

The stability of nanocomposites is a major issue of concern. This study examined the stability of the nanocomposite by sonicating a suspension of the *Ag*-SnO_2 nanocomposites in water for one hour. The centrifuged solution was then analyzed for the leached AgNPs using a UV-visible spectrophotometer (Fig. S15). The AgNPs showed no absorbance peak (Fig. S15). The reusability of *Ag*-SnO_2 was tested by centrifuging the catalyst from the dye solution, followed by washing with DI water and drying in an air oven at 100 °C. The reused catalyst showed a similar response (Fig. S16a and S16b) to that of the fresh catalyst, highlighting the stability and reusability of the *Ag*-SnO_2 nanocomposites.

Conclusions

Ag-SnO_2 nanocomposites with different concentrations of silver precursor (1 mM and 3 mM) were synthesized using an EAB without toxic chemicals, surfactants and organic solvents. Compared to pure SnO_2 the *Ag*-SnO_2 nanocomposites showed enhanced photocatalytic performance for the photodecomposition of MO, MB, 4-NP and 2-CP under visible light irradiation. The enhanced photocatalytic activities of *Ag*-SnO_2 were attributed mainly to the introduction of AgNPs, which facilitated charge separation of the photogenerated electrons and holes. The anchoring of AgNPs on the *p*-SnO_2 surface improves the separation and transfer of charge carriers under visible light irradiation, through which the visible light photoactivity of the *Ag*-SnO_2 nanocomposites were enhanced.

The photoelectrochemical (EIS, LSV and DPV) response highlighted the enhanced photoactivity of the *Ag*-SnO_2 nanocomposites under visible light irradiation. This study establishes a simple and green method for preparing highly visible light-active *Ag*-SnO_2 nanocomposite materials for possible applications in industrial effluent treatment and photoelectrode materials. This environmentally friendly synthesis is expected to provide a new means of synthesizing a series of metal-metal oxide photocatalysts for use in photo-assisted catalytic reactions.

Acknowledgements

This study was supported by the 2013 Yeungnam University Research Grant, South Korea.

Notes and references

School of Chemical Engineering, Yeungnam University, Gyeongsan-si, Gyeongbuk 712-749, South Korea. Phone: +82-53-810-2517; Fax: +82-53-810-4631,
***Email:** mhcho@ynu.ac.kr*

†Electronic Supplementary Information (ESI) available: [DRS spectra of *p*-SnO_2 and *Ag*-SnO_2, TEM and HRTEM images of the *p*-SnO_2, SAED, HAADF and EDX of *p*-SnO_2 and *Ag*-SnO_2, C1s spectra of *p*-SnO_2 and *Ag*-SnO_2, Photodegradation spectra of MO, MB, 4-NP and 2-CP, UV-Vis spectra of *Ag*-SnO_2 for Ag leaching and recycled photodegradation plots of MO and MB] See DOI: 10.1039/b000000x/

1. A. Fujishima, K. Honda, *Nature,* 1972, **238**, 37–38.
2. S. A. Ansari, M. M. Khan, M. Omaish, J. Lee and M. H. Cho, *J. Phys. Chem. C* 2013, **117**, 27023−27030.
3. S. H. S. Chan, T. Y. Wu, J. C. Juan and C. Y. Teh, *J. Chem. Technol. Biotechnol.*, 2011, **86**, 1130–1158.
4. H. Chen, C. E. Nanayakkara and V. H. Grassian, *Chem. Rev.*, 2012, **112**, 5919–5948.
5. M. M. Hassan, W. Khan, A. Azam, A.H. Naqvi, *J. Lumin.*, 2014, **145**,160–166.
6. S. A. Ansari, M. M. Khan, M. Omaish, J. Lee and M. H. Cho, *New J. Chem.* 2014, **38**, 2462–2469.
7. Z. Zhao, H. Tan, H. Zhao, Y. Lv, L. Zhou and Y. Song, *Chem. Commun.*, 2014, **50**, 2755-2757.
8. R. Saravanan, N. Karthikeyan, V. K. Gupta, E. Thirumal, P. Thangadurai, V. Narayanan, *Mater. Sci. Eng., C,* 2013, **33**, 2235–2244.
9. P. Wang, B. Huang, Y. Dai, M. H. Whangbo, *Phys Chem Chem Phys,* 2012, **14**, 9813–9825.
10. L. Jing, W. Zhou, G. Tian and H. Fu, *Chem. Soc. Rev.*, 2013, **42**, 9509–9549.
11. S.T. Kochuveedu, Y. H. Jang and D. H. Kim, *Chem. Soc. Rev.*, 2013, **42**, 8467–8493.
12. M. M. Khan, S. A. Ansari, M. O. Ansari, B. K. Min, J. Lee and M. H. Cho, *J. Phys. Chem. C,* 2014, **118**, 9477−9484.
13. S. A. Ansari, M. M. Khan, J. Lee, M. H. Cho, *J. Ind. Eng. Chem.*, 2014, 20, 1602–1607.
14. J. Ran, J. Zhang, J. Yu, M. Jaroniec and S. Z. Qiao, *Chem. Soc. Rev.*, 2014, DOI: 10.1039/C3CS60425J.
15. Z. Khan, T. R. Chetia, A. K. Vardhaman, D. Barpuzary, C. V. Sastri and M. Qureshi, *RSC Adv.*, 2012, **2**, 12122–12128.
16. C. M. Fan, Y. Peng, Q. Zhu, L. Lin, R. X. Wang and A. W. Xu, *J. Phys. Chem. C*, 2013, **117**, 24157–24166.
17. W. Wu, L. Liao, S. Zhang, J. Zhou, X. Xiao, F. Ren, L. Sun, Z. Dai and C. Jiang, *Nanoscale*, 2013, **5**, 5628–5636.
18. H. J. You, R. Liu, C.C. Liang, S.C. Yang, F. Wang, X.G. Lu, B.J. Ding, *J. Mater. Chem. A,* 2013, **1,** 4097–4104.
19. S. Kalathil, M. M. Khan, J. Lee and M. H. Cho, *Biotechnol. Adv.,* 2013, **31**, 915–924.
20. M. M. Khan, S. A. Ansari, J. H. Lee, J. Lee and M. H. Cho, *ACS Sustainable Chem. Eng.* 2014, **2**, 423–432.
21. T. H. Han, M. M. Khan, S. Kalathil, J. Lee, M. H. Cho, *Ind. Eng. Chem. Res.*, 2013, **52**, 8174−8181.
22. J. Liqiang, Q. Yichun, W. Baiqi, L. Shudan, J. Baojiang, Y. Libin, F. Wei, F. Honggang and S. Jiazhong, *Sol. Energy Mater. Sol. Cells,* 2006, **90**, 1773–1787.
23. C. C. Zheng, Y. Z. Y, L. X, Z. Q, W. K, *Dalton Trans.,* 2011, **40**, 9566–9570.
24. G. Wang, X. Wang, J. Liu and X. Sun, *Chem. Eur. J.* 2012, **18**, 5361–5366.
25. N. N. Rao, A. K. Dubey, S. Mohanty, P. Khare, R. Jain and S. N. Kaul, *J. Hazard. Mater.*, 2003, **101**, 301–314.
26. C. Clavero, *Nature Photonics,* 2014, **8**, 95–103.
27. Z. Chen, L. Fang, W. Dong, F. Zheng, M. Shen and J. Wang, *J. Mater. Chem. A*, 2014, **2**, 824–832.
28. M. Qamar and A. Khan, *RSC Adv.*, 2014, **4**, 9542–9550.
29. R. W. Murray, *Chem. Rev.*, 2008, **108**, 2688–2720.
30. S. Kalathil, J. Lee and M. H. Cho, *J. Nanopart. Res.,* 2013, **14**, 1051–1060.
31. M. M. Khan, S. A. Ansari, J. Lee, M. H. Cho, *J. Ind. Eng. Chem.*, 2013, 19, 1845–1850.
32. X. Bai, L. Wang, R. Zong, Y. Lv, Y. Sun and Y. Zhu, *Langmuir*, 2013, **29**, 3097−3105.
33. L. Zhao, L. Fang, W. Dong, F. G. Zheng and M. R. Shen, *Appl. Phys. Lett.*, 2013, **102**, 121905.
34. Y. Lv, Y. Zhu, and Y. Zhu, *J. Phys. Chem. C*, 2013, **117**, 18520−18528.
35. W. H. Leng, Z. Zhang, J. Q. Zhang and C. N. Cao, *J. Phys. Chem. B,* 2005, **109**, 15008–15023.
36. J. Gan, X. Lu, J. Wu, S. Xie, T. Zhai, M. Yu, Z. Zhang, Y. Mao, S. C. Wang, Y. Shen and Y. Tong, *Sci. Rep.*, 2013, **3**, 1021–1028.
37. S. A. Ansari, M. M. Khan, M. O. Ansari, S. Kalathil, J. Lee and M. H. Cho, *RSC Adv.*, 2014, **4**,16782–16791.
38. M. M. Khan, S. A. Ansari, D. Pradhan, M. Omaish, D. H. Han, J. Lee and M. H. Cho, *J. Mater. Chem. A*, 2014, **2**, 637–644.
39. H. M. Chen, C. K. Chen, C. J. Chen, L. C. Cheng, P. C. Wu, B. H. Cheng, Y. Z. Ho, M. L. Tseng, Y. Y. Hsu and T. S. Chan, *ACS Nano*, 2012, **6**, 7362–7372.
40. M. O. Ansari, M. M. Khan, S. A. Ansari, K. Raju, J. Lee and M. H. Cho, *ACS Appl. Mater. Interfaces,* 2014, DOI: 10.1021/am500488e.
41. M. M. Khan, S. A. Ansari, D. Pradhan, D. H. Han, J. Lee and M. H. Cho, *Ind. Eng. Chem. Res.*, 2014**,** DOI: 10.1021/ie500986n.

